JOURNAL OF MATERIALS SCIENCE 30 (1995) 2455–2462

Influence of spherical indentor radius on the indentation-induced transformation behaviour of silicon

E. R. WEPPELMANN*, J. S. FIELD, M. V. SWAIN
CSIRO, Division of Applied Physics, Lindfield, New South Wales 2070, and Department of Mechanical and Mechatronics Engineering, University of Sydney, New South Wales 2006, Australia

The force–displacement records of the indentation of silicon single crystals have been monitored with an ultra-micro indentation system using spherical-tipped diamond indentors. The observations with indentors of different radii varying from nominally 5–20 μm all exhibited similar behaviour. At low loads, the behaviour was entirely elastic and exhibited complete reversibility. At slightly heavier loads the onset of non-linear behaviour occurred, which, in many cases, appeared to be completely reversible. In all the other cases at this and higher load levels, a "pop-out" event occurred during the unloading in what otherwise appeared to be an elastic unloading. The results are interpreted in terms of the indentation pressure-induced phase transformation from silicon-I to silicon-II on loading and to silicon-III upon unloading.

1. Introduction

There has been considerable interest in the indentation of silicon for many years. Early work by Goryunova *et al.* [1] and Gridneva *et al.* [2] suggested that a phase change took place beneath the contact site which caused the silicon to change from semiconducting to metallic-like behaviour. More recently, there has been further support for this premise by Clarke and co-workers [3–6]. These authors, using pointed indentors, suggested that the "pop-out" event occurring during unloading was a consequence of the silicon-II to silicon-III phase transformation and its accompanying volumetric expansion. However, because of the difficulties of analysing the pointed indentation force–displacement data and the inevitability of cracking about such indentations, the "pop-out" events could only be described qualitatively.

Gilman [7] extended his previous work on the relationships between hardness in semi-conducting materials and the bandgap. The basis of these newer predictions was that the semi-conducting behaviour of silicon (and other III–IV and II–VI compounds) vanished when the pressure dependence of the dielectric behaviour of the materials becomes unstable. This is the so-called Hertzfield transition pressure.

Independent assessment of the pressure dependence of the phase transitions of silicon has been addressed by many authors using high-pressure (diamond anvils and hydrostatic pressure cell) devices. Hu and co-workers [8, 9] have quantified the phase-transformation pressures, the unit cell structures and volumes for the various phase changes silicon undergoes upon loading and unloading. It is generally agreed that at a pressure of 11–13 GPa, the familiar diamond cubic form of silicon (silicon-I) transforms to a denser β-tin structure (silicon-II) with a resulting 22% reduction in volume. Upon unloading, the silicon-II undergoes another phase change to a bcc structure known as silicon-III, with an intermediate density between silicon-I and silicon-II; the unit cell volume is some 8% more dense than the silicon-I phase. The reverse transformation is proposed to occur at a pressure between 8.5 and 10.8 GPa.

High-resolution transmission electron microscopy (TEM) of the material directly under a pointed indentation performed by Page *et al.* [10] established that material of amorphous and higher density developed in this region. More recently, Clarke [11] using TEM has observed evidence of the silicon-III phase within the remnant indentation-deformed zone. In another development, the present authors [12] used an 8.5 μm tipped spherical indentor to investigate the behaviour of silicon and were able to identify the pressure for the onset of the silicon-I to silicon-II phase transformation as well as the silicon-II to silicon-III phase-transformation pressure upon unloading. The present paper is an extension of that work and compares the behaviour of indentation tests carried out with indentors of different radii. The results are also discussed in terms of the indentation size effect which has been reported for silicon by a number of authors [13–15].

* *Present address*: IMF-II/IZSM, KfK, Karlsruhe 76021, Germany.

0022–2461

2. Theory

The contact of a sphere on to an elastic half space is illustrated in Fig. 1. The total depth of penetration is given by Johnson [16] as

$$\delta = \Phi m \tag{1}$$

where

$$\Phi = (3P/4E^*)^{2/3} \tag{2}$$

and

$$m = (1/R)^{1/3} \tag{3}$$

In these expressions, P is the load, R is the radius of the indentor, and

$$1/E^* = (1 - \nu_m)/E_m + (1 - \nu_i)/E_i \tag{4}$$

in which ν_m and E_m are Poisson's ratio and Young's modulus for the material of the half space, and ν_i and E_i are Poisson's ratio and Young's modulus for the indentor material, respectively.

In the case of elastic contact, Sneddon [17] showed that the displacements of a plane surface above and below the circle of contact are equal. Consequently, for penetrations that are small compared with the radius of a spherical indentor tip, the relationship between the elastic depth of penetration and the radius of the circle of contact is approximately

$$\delta = a^2/R \tag{5}$$

and the mean pressure over the contact circle is

$$p_m = P/\pi a^2 \tag{6}$$

Combining the above two equations leads to the simple expression between contact pressure and measured displacements, namely

$$p_m = P/\pi\delta R \tag{7}$$

In the previous papers, the authors extended the above analysis to elastic–plastic loading [12, 18]. Such an approach enabled a simple expression for the complete unloading response and thereby to determine unequivocally the plastic penetration depth at maximum load and the maximum mean contact pressure. The former study also enabled the elastic modulus to be monitored by partial unloading steps throughout the course of the test. The second paper extended this analysis to silicon and showed an approach to estimate and simulate the complete load–displacement response for silicon. In this paper, these details will not be reproduced; rather the essential features will be drawn upon and mentioned in Section 4.

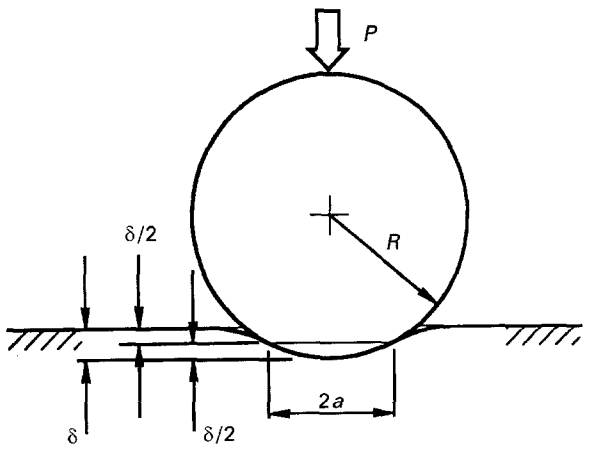

Figure 1 Schematic diagram of the elastic loading of a sphere on a flat.

3. Experimental procedure

3.1. Materials

All the indentation tests were carried out on high-purity commercially available silicon discs, cut and polished such that the indented surface was aligned parallel to the [1 0 0] orientation of the single crystal. They were p-doped with a resistivity of 0.05–0.08 Ω cm and had a thickness of 1.05 mm. The surface roughness of the silicon was determined using a Wyko digital phase shifting optical interferometer which has a lateral spatial resolution of 1 μm and a vertical resolution of 1 nm. The roughness was found to be always smaller than 4 nm, peak to valley.

3.2. Spherical indentors

In this study, commercially available diamond-tipped spherical indentors, obtained from Synton, were used to conduct the tests. Prior to usage the shape of the indentors was evaluated using the SEM and a profilometer. Scanning electron micrographs of the contours of the indentors were taken from four different orientations. These micrographs were evaluated by fitting thin concentric circle templates to each contour of the tip region. The radius of each indentor was then obtained by averaging these measurements. The results agreed well with the measurements of the radii as carried out with the profilometer.

Scanning electron micrographs of the tip region of the indentors used in this study are shown in Fig. 2a–c. None of these indentors was what might be termed "perfect". The nominal 5 μm radius indentor shown in Fig. 2a has a tip radius which is very close to the nominal radius, but has an abrupt transition from the spherical to the conical region. Consequently, the useful penetration depth under the contact region is restricted to only some 700 nm for the spherical-shaped region of the indentor. Beyond this depth, the force–displacement behaviour is more adequately modelled by a sphero-conical indentor.

The actual tip of the nominal 10 μm radius indentor shown in Fig. 2b is also not perfect, the radius differing slightly depending on the penetration depth during contact. For very shallow penetration depths, the actual radius is about 8.5 μm. As the penetration depth increases, the radius also increases until the nominal value of 10 μm is reached at a depth of ~ 3 μm. The blend from the spherical to conical region is almost perfect, which enables the spherical portion of the tip to be used up to an indentation depth of ~ 3.5 μm.

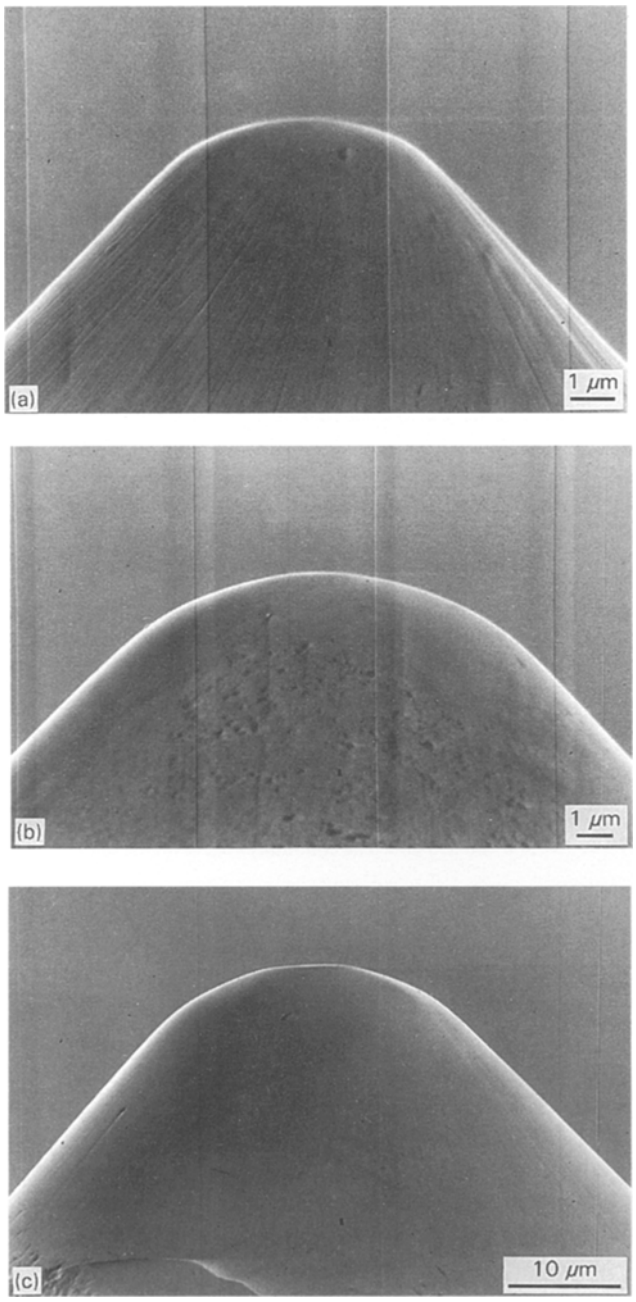

Figure 2 Scanning electron micrographs of the spherical indentors used in this study; (a) 5 μm indentor, (b) 10 μm indentor, and (c) 20 μm indentor.

The nominal 20 μm radius-tipped indentor exhibits some major deviations from a spherical shape as shown in Fig. 2c. The tip region appears to have an almost flat area of ~ 7μm diameter sitting somewhat on the top of the sphere. The overall radius of this indentor, i.e. the radius for the entire spherical portion, was measured to be ~ 22 μm. At shallow depths of penetration, less than 500 nm, the appropriate radius was ~ 28–30 μm.

Despite the above efforts of evaluating the radii of the spherical-shaped indentors, it must be admitted that the actual radius at the very first contact region, that is for penetration depths of around 1% of the nominal tip radius, may not be measurable with sufficient accuracy. This situation is a consequence of the fact that at the very tip region, minute deviations in the polishing process and the associated roughness, as well as that of the substrate surface roughness, will lead to major deviations of the actual or effective tip radius.

3.3. Indentation measurements

All the indentation tests were carried out using the ultra-micro indentation system UMIS-2000 which is described in detail elsewhere [19].

With the nominal 5 μm radius indentor, tests were carried out at various loads between 12.5 and 100 mN at every 12.5 mN and between 125 and 400 mN at every 25 mN. At loads less than or equal to 100 mN, 100 load steps were used upon loading and unloading. At higher loads only 50 load steps were used. Using the nominal 10 μm radius indentor, measurements were carried out at loads ranging from 70–130 mN at 15 mN intervals and then at 150, 200, 350, 500, 650 and 800 mN. At loads less than or equal to 200 mN, 100 load steps were used, whereas only 50 load steps were used at higher loads. With the nominal 20 μm radius indentor, tests were carried out at 100, 200, 350, 500, 650 and 800 mN, always using 100 steps on both loading and unloading.

Except for indentations made with the 20 μm radius indentor, five indentation tests were produced at each load. With the 20 μm radius indentor, only three indentations were carried out at each load. All indentations were placed 70–100 μm apart from each other.

4. Observations and discussion

4.1. Observations with the nominal 5 μm indentor

The force–displacement records of the indentations made with the 5 μm indentor are shown in Fig. 3a–d. All of the five measurements made at 25 mN maximum load were entirely elastic (see Fig. 3a). The first evidence of *plastic* behaviour was found at some of the indentations carried out at 37.5 mN as the unloading curves were slightly offset from the loading data. The hysteretic behaviour became more distinct during the indentations made at 50 mN. Four of the five force–displacement records obtained at this load exhibited a perfectly closed hysteresis loop. The averaged data of these measurements are shown in Fig. 3b.

All indentation tests which were carried out at loads in excess of 50 mN more clearly exhibited the "pop-out" phenomena during unloading. Examples of the force–displacement data at these heavier loads are shown in Fig. 3c and d. Superimposed on all the force–displacement data is the anticipated elastic response assuming no plastic deformation. The transition from elastic to plastic behaviour is marked with an arrow. Observations of the residual impressions with the SEM revealed that fracture initiation seems to occur at loads of 175 mN. Typical observations of the deformation and cracking at various loads are shown in Fig. 4. At a load of 200 mN (Fig. 4a) the contact region is clearly defined and small radial

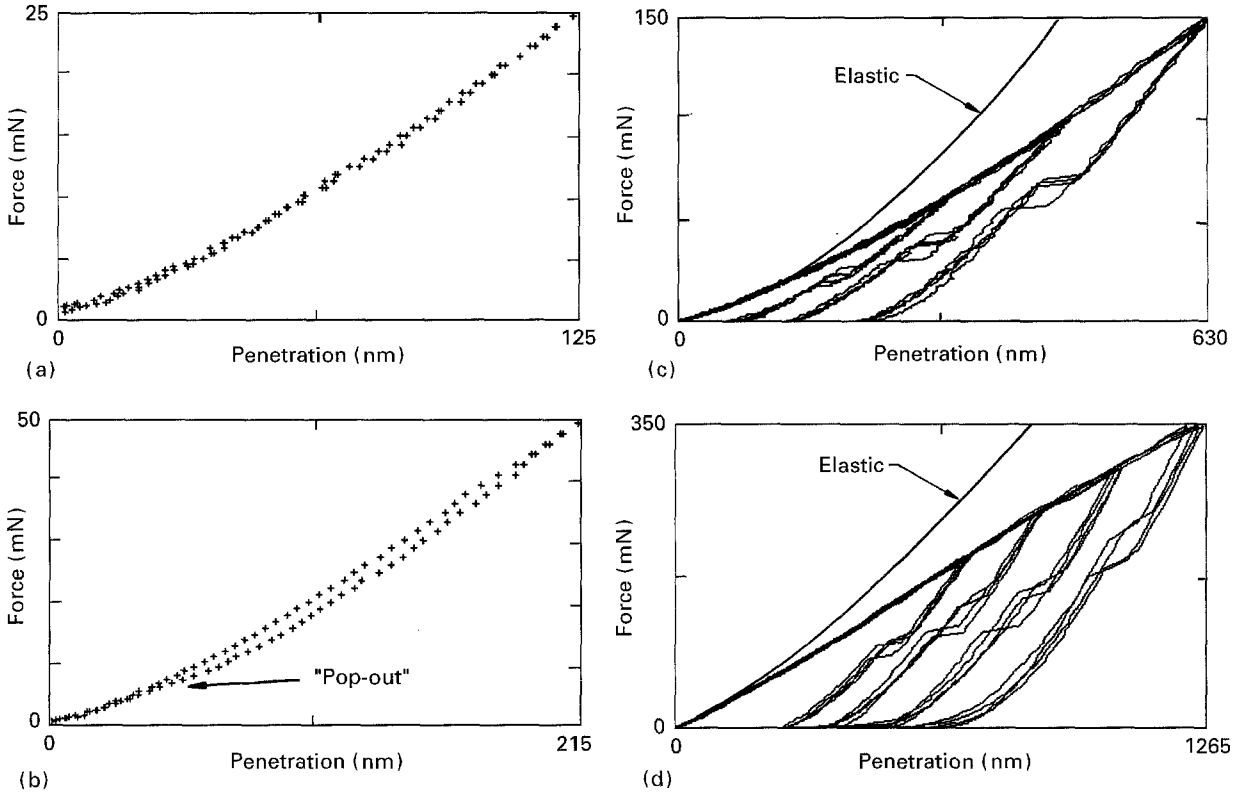

Figure 3 Force–displacement data carried out on silicon with a nominal 5 μm indentor at loads of (a) 25 mN, average of five measurements, (b) 50 mN, average of four measurements, (c) 62.5, 100 and 150 mN and (d) 200, 250, 300 and 350 mN. The continuous curve on the data is the elastic response anticipated from Equations 1–4.

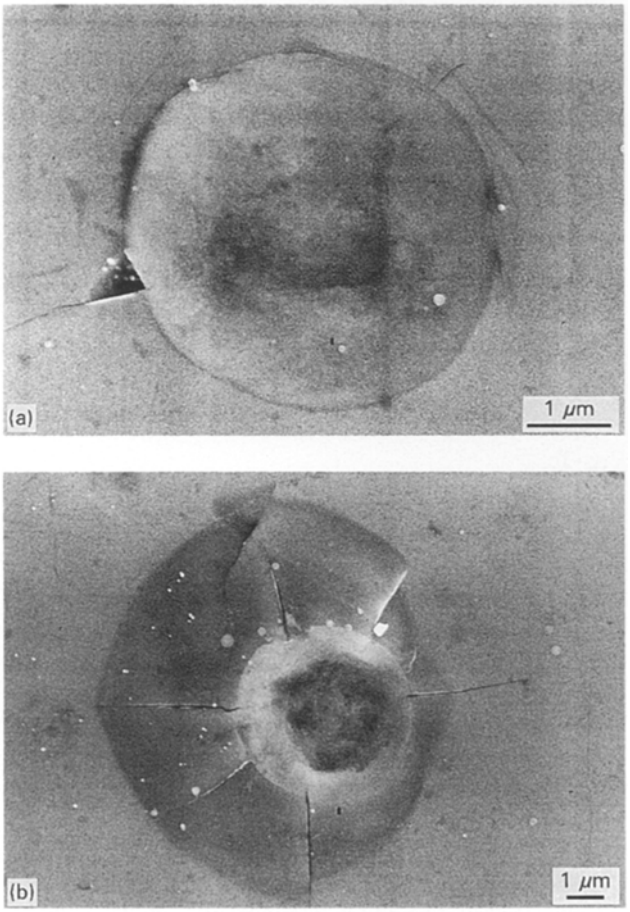

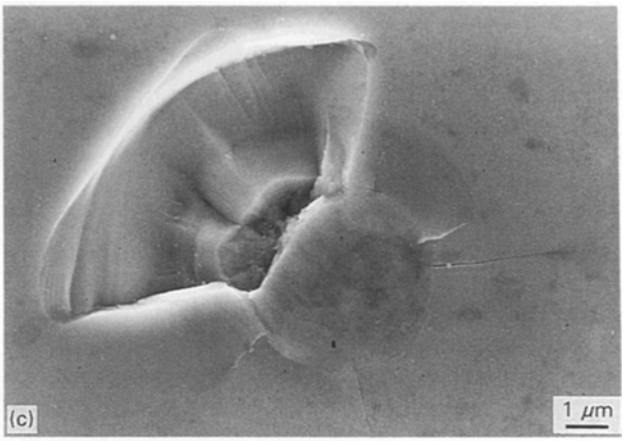

Figure 4 Scanning electron micrographs of the residual impression and associated cracking with (a) 200 mN, (b) 250 mN and (c) 350 mN force applied to the 5 μm radius indentor.

cracks are seen to emanate from the contact periphery, whereas for heavier loads, 250 mN (Fig. 4b) and 350 mN (Fig. 4c), the extent of deformation and cracking becomes increasingly more substantial.

4.2. Observations with the nominal 10 μm indentor

Examples of the force–displacement curves are shown in Fig. 5a–d. The deformation was entirely elastic up

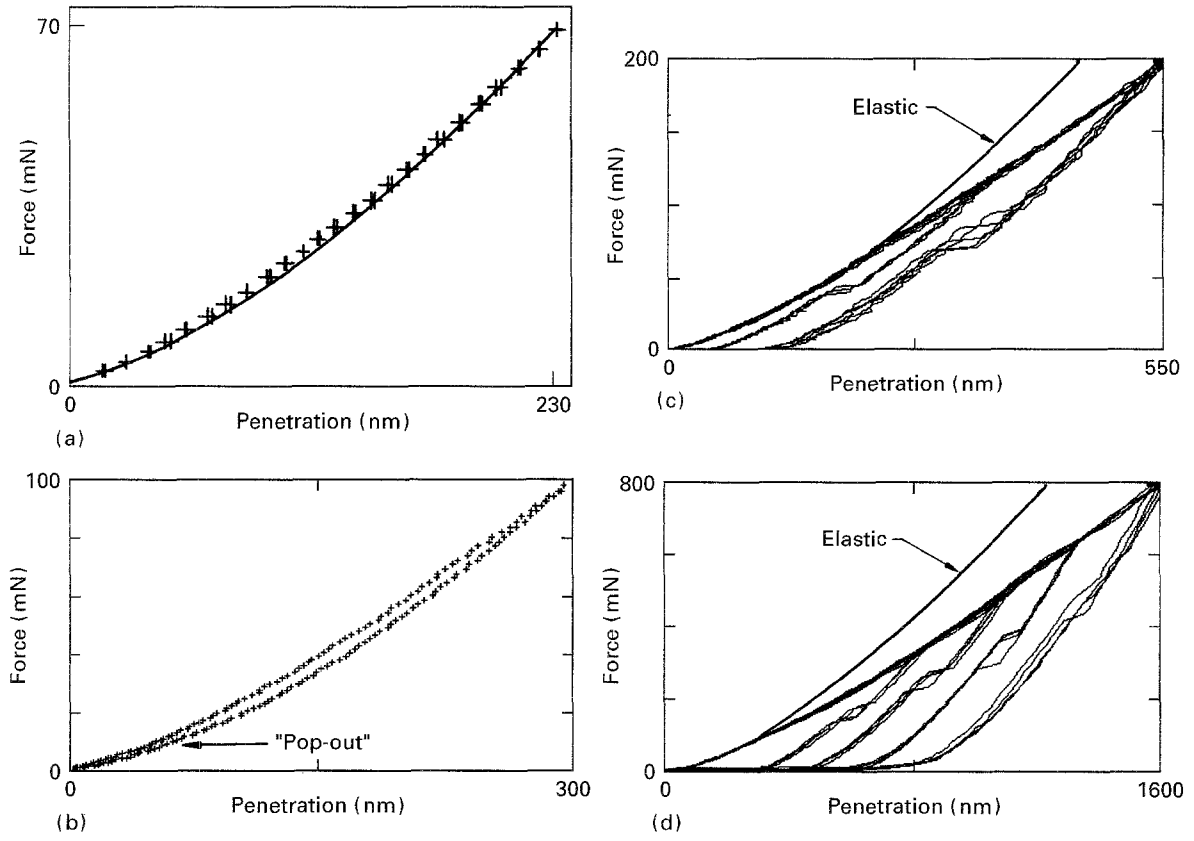

Figure 5 Force–displacement data on single-crystal silicon obtained with a nominally 10 μm spherical indentor at loads of (a) 70 mN, (b) 100 mN, (c) 130 and 200 mN, and (d) 350, 500, 650 and 800 mN.

to a load of 70 mN, Fig. 5a. Four of the indentations made at 85 mN exhibited slight evidence of plastic flow, indicating that the onset of permanent deformation occurred between 70 and 85 mN. The fifth force–displacement record still exhibited an entirely elastic behaviour. The hysteretic behaviour became more distinct with indentation tests carried out at 100 mN. Four of the five force–displacement records obtained at this load exhibited a perfectly closed hysteresis loop. The reverse transformation of these indentations does not show any "pop-out" phenomena during the unloading. The fifth displacement curve of the five indentation tests carried out at this load exhibited a first "pop-out" during the unloading (see Fig. 5b).

Representative examples of the force–displacement data at heavier loads are shown in Fig. 5c for indentations made at 130 and 200 mN maximum load. Fig. 5d shows the results of indentation tests carried out at 350, 500, 650 and 800 mN maximum loads. These force–displacement curves exhibit an apparent plastic behaviour as well as a distinctive "pop-out" step during unloading. In order to determine whether fracture or plastic deformation is responsible for this behaviour, the indentations were examined using a scanning electronic microscope (SEM).

Typical observations of the fracture patterns about heavier loaded impressions are shown in Fig. 6a–c. These observations clearly indicate that radial and lateral cracks are forming, although there is some evidence that the lateral cracks may have initiated from a Hertzian cone crack (see Fig. 6a, where a circular ring crack around the area of contact can be observed; see also Fig. 6b where a Hertzian cone crack is formed). Observations of the lower load impressions revealed that only one of the five indentations at 350 mN exhibited a small radial crack. These observations indicate that *fracture* does not occur during indentation tests if the maximum load is smaller than 350 mN. Consequently, the deformation of the silicon under the indentor is caused by some kind of *plastic* behaviour.

4.3. Observations with the nominal 20 μm indentor

Fig. 7a and b show force–displacement records obtained on the silicon disc using the nominally 20 μm radius indentor. All indentations made at loads less than or equal to 650 mN were entirely elastic (see Fig. 7a). The reason why the elastic region is extended up to this high loads lies in the fact that the actual tip of this indentor is a slightly inclined plane with a diameter of around 7 μm. The equivalent radius of this indentor is estimated to be $\sim$ 28 μm (see Fig. 2c). All the indentations made at 800 mN exhibited a limited hysteretic behaviour with a clear distinctive "pop-out" during the unloading (see Fig. 7b).

4.4. Analysis of the force–displacement data

As mentioned in Section 2, only a simple basis for analysis of the force–displacement data will be presented here. The force for the onset from elastic to

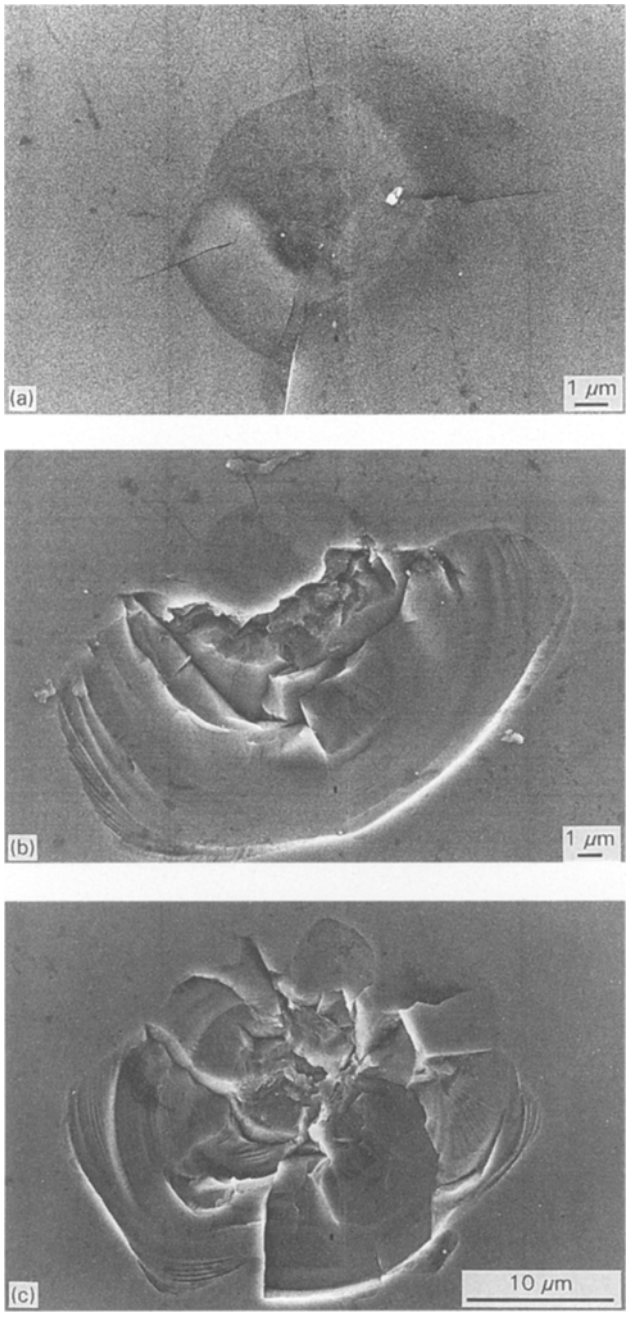

Figure 6 Scanning electron micrographs of the deformation and cracking produced about indentations with the 10 μm radius indentor at maximum loads of (a) 500 mN, (b) 650 mN, and (c) 800 mN.

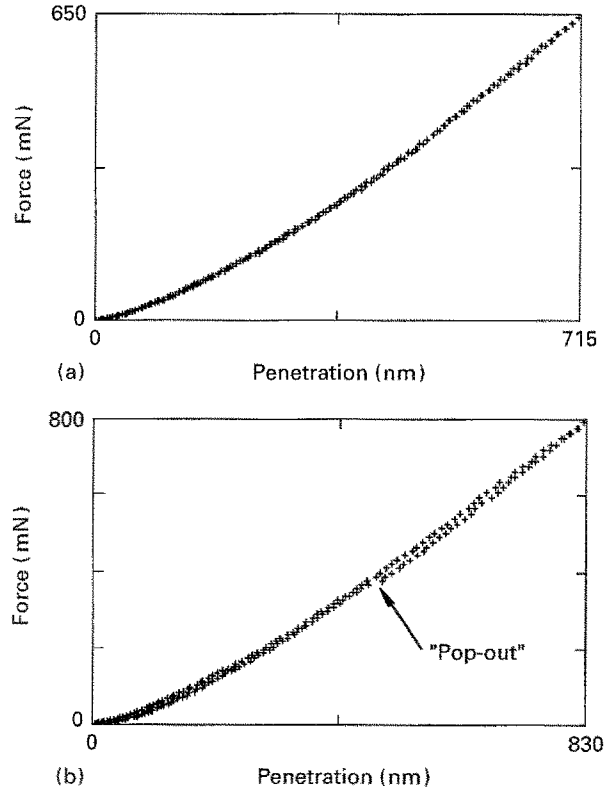

Figure 7 Force–displacement data on single-crystal silicon obtained with the nominally 20 μm radius indentor at loads of (a) 650 mN, and (b) 800 mN.

TABLE I Critical phase-transformation pressures

Radius R (μm)		Critical Load, P (mN)	Displacement δ (nm)	Contact pressure, p_m (GPa)
Nominal	Actual			
5	5	37 ± 4	189 ± 6	12.5 ± 1.1
10	8.5	78 ± 7	264 ± 15	11.1 ± 1.0
20	28	743 ± 18	713 ± 40	11.8 ± 1.1

"plastic" behaviour is marked on the force–displacement curves and from these values the mean contact pressure may be estimated from Equation 7. However, because the actual contact or detectable force of the measurement system is always greater than zero, an additional displacement to account for this must be added to the measured value. The simplest means of estimating this additional displacement is to extrapolate δ proportional to $P^{2/3}$ (Equations 1 and 2) to zero force. The estimated critical force and displacement values at the onset of "plastic" deformation are 37 ± 4 mN and 172 ± 6 nm for the nominally 5 μm (actual $R = 5$ μm) radius indentor, 78 ± 7 mN and 250 ± 15 nm for the nominally 10 μm (actual $R = 8.5$ μm) indentor, and 683 ± 18 mN and 705 ± 40 nm for the nominally 20 μm (actual $R = 28$ μm) indentor. The contact force for these measurements was ~ 0.6 mN which implies that the additional displacements that must be added to the above displacement values are 17, 14 and 8 nm, respectively. Inserting these values into Equation 7 leads to the estimates shown in Table I of the critical contact pressure for the silicon-I to silicon-II phase transformation.

4.5. Simulation of the force–displacement data

As discussed in the previous paper [12], the interpretation of the force–displacement data may be considered in terms of the pressure-induced phase transformation from silicon-I to silicon-II on loading and silicon-II to silicon-III during unloading. This transformation takes place within the hydrostatic compressive zone beneath the indentor. In this section, one of the force–displacement curves for each indentor will be simulated.

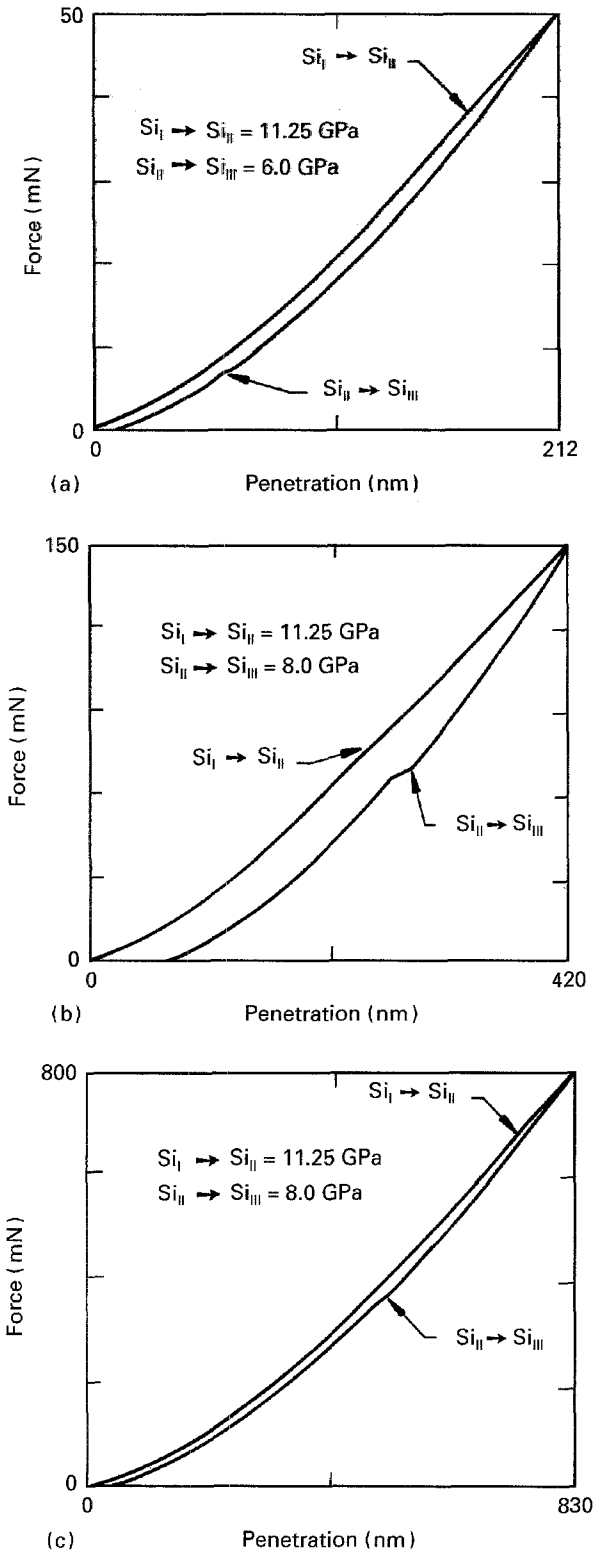

Figure 8 Simulations of the force–displacement response of silicon to indentations made with (a) a 5 μm indentor to a maximum force of 50 mN, (b) a 8.5 μm indentor to 150 mN, and (c) a 28 μm indentor to 800 mN.

A simple program to simulate the data was written to evaluate initially the elastic displacement up to the critical contact pressure for the onset of the phase transformation. At heavier loads it was assumed that the mean contact pressure remained constant until the peak load was achieved. The displacement at each loading step was calculated in the manner outlined by Field and Swain [18] for metallic elastic–plastic materials assuming no work-hardening occurred. During unloading, the initial response was elastic and the mean contact pressure was calculated for each unloading step until the pressure equals the silicon-II to silicon-III phase-transformation pressure. The extent of "pop-out" at this pressure is dependent upon the ratio of the densities, ρ, of the silicon-II and silicon-III phases. The values chosen were $\rho_{II} = 2.84 \times 10^3\ kg\,m^{-3}$ and $\rho_{III} = 2.52 \times 10^3\ kg\,m^{-3}$. For all the simulations the values of the elastic modulus of silicon-I and the transformation pressure for the silicon-I to silicon-II transition were kept constant at 170 and 11.5 GPa, respectively. The pressure for the silicon-II to silicon-III phase transformation during unloading was adjusted to fit the observations. Examples of simulations for each of the three indentors with peak loads of 50, 150 and 800 mN, respectively, are shown in Fig. 8a–c. The actual radii of the indentors and the silicon-II to silicon-III transformation pressures used in the simulation are listed in the respective figures. The simulations should be compared with the actual results in Figs 3b, 5c and 7d. It can be seen that the modelled curves agree well with the measured results.

The present observations and analysis with spherical indentors do not support the previous observations for an indentation size effect (ISE) as widely reported using Vickers indentors [13, 14]. There is, however, some controversy in the case of silicon, as Roberts [14] has reported to have seen a positive ISE effect for silicon whereas Feltham and Banerjee [15] have reported a negative ISE (that is, increasing hardness with load). Li and Bradt [20] have recently re-analysed the data of Feltham and Banerjee and suggest that the increasing hardness with load is a consequence of indentation cracking about the impression. Another recent study by Pharr *et al.* [21] using a Berkovich indentor over a range of load from 1–115 mN and actually measuring the indentation dimensions with an SEM, reported nearly constant hardness with depth. The present results support the observations of Pharr *et al.* [21] but suggest that spherical-tipped indentors are far superior for investigating the various stages of the *elastic/plastic* deformation of these brittle materials, than pointed indentors.

5. Conclusions

The present study has shown that the elastic–"plastic" response of silicon appears to be essentially independent of spherical indentor radius over the range investigated. Spherical indentors enable a complete characterization of the critical phase-transformation pressures of silicon during loading and unloading which are in very good agreement with literature values. There appears to be no convincing evidence for any indentation size effect using this approach.

Acknowledgements

The authors thank J. Mencik and P. Martin for their comments on the manuscript.

References

1. N. A. GORYUNOVA, A. S. BORSHCHERSKII and C. N. TRETIAKOV, "Physics of III–V Compounds. Semi-Conductors and Semi-metals" (Academic Press, San Diego, 1968) Ch. 1.
2. I. V. GRIDNEVA, YU. V. MILMAN and V. I. TREFILEV, *Phys. Status. Solidi* **9**(14) (1972) 177.
3. D. R. CLARKE, M. C. KNOLL, P. D. KIRCHENER, R. F. COOK and B. J. HOCKEY, *Phys. Rev. Lett.* **21** (1988) 2156.
4. G. M. PHARR, W. C. OLIVER and D. R. CLARKE, *Scripta Metall* **23** (1989) 1949.
5. *Idem, J. Elect. Mater.* **19** (1990) 881.
6. G. M. PHARR, in "Thin Films: Stresses and Mechanical Properties III", edited by W. D. Nix, J. C. Bravman, E. Arzt and L. B. Freund (Materials Research Society Symposia Proceedings, Pittsburgh, PA, 1992) **239**, p. 301.
7. J. J. GILMAN, *J. Mater. Res.* **7** (1992) 535.
8. J. Z. HU and I. L. SPAIN, *Solid State Commun.* **51** (1983) 263.
9. J. Z. HU, L. D. MERKLE, C. S. MENONI and I. L. SPAIN, *Phys. Rev.* **B34** (1986) 4679.
10. T. F. PAGE, W. C. OLIVER and C. J. McHARGUE, *J. Mater. Res.* **7** (1992) 450.
11. D. R. CLARKE, private communication (1993).
12. E. R. WEPPELMANN, J. S. FIELD and M. V. SWAIN, *J. Mater. Res.* **8** (1993) 830.
13. P. M. SARGENT, in "Micro-indentation Techniques in Materials Science and Engineering", edited by P. J. Blau and B. R. Lawn, ASTM STP 889 (American Society for Testing and Materials, Philadelphia, PA 1984) p. 160.
14. S. G. ROBERTS, PhD thesis, Cambridge University (1973).
15. P. FELTHAM and R. BANERJEE, *J. Mater. Sci.* **27** (1992) 1626.
16. K. L. JOHNSON, "Contact Mechanics" (Cambridge University Press, Cambridge, 1985).
17. I. N. SNEDDON, *Proc. Cambr. Philos. Soc.* **44** (1949) 429.
18. J. S. FIELD and M. V. SWAIN, *J. Mater. Res.* **8** (1992) 297.
19. T. J. BELL, A. BENDELI, J. S. FIELD, M. V. SWAIN and E. G. THWAITE, *Metrologia* **28** (1991/92) 463.
20. H. LI and R. C. BRADT, private communication (1994).
21. G. M. PHARR, W. C. OLIVER and D. S. HARDING, *J. Mater. Res.* **6** (1991) 1129.

Received 5 July
and accepted 31 October 1994